



Crustal Stress in the Northern Red Sea Region as Inferred from Seismic *b*-values, Seismic Moment Release, Focal Mechanisms, Gravity, Magnetic, and Heat Flow Data

Ali K. Abdelfattah^{1,2} · Chokri Jallouli^{1,3} · Saleh Qaysi¹ · Basem Al-Qadasi¹

Received: 6 March 2020 / Accepted: 2 July 2020 / Published online: 28 July 2020
© Springer Nature B.V. 2020

Abstract

This study explores the spatial distribution of seismicity, the pattern of *b*-values, gravity and magnetic anomalies, heat flow data, and focal mechanism solutions to more thoroughly understand the present-day stress distribution and the nature of the crust, which characterize the rifting process in the northern Red Sea region. The region shows alternating low and high *b*-values in congruence with low and high cumulative seismic moment releases, respectively, and with negative and positive gravity anomalies, respectively. In general, except for larger-sized earthquake locations that characterized by high stress accumulation, low *b*-values, low seismic moment release, and low-gravity anomalies dominate the zones of the Gulf of Aqaba and the Gulf of Suez, thereby implying low stress accumulation consistent with an old crust of no differential development. Conversely, the rest of the Northern Red Sea region exhibited heterogeneities in the spatial distribution of *b*-values, cumulative seismic moment releases, and gravity anomalies, thereby implying stress heterogeneities. The stress heterogeneities may impute to the differences in material properties of the upper crust in the region. Zones of a positive Bouguer anomaly and high stress are notably associated with a relatively weak crust characterized by high rate of seismicity, while zones of the negative Bouguer anomaly and low stress characterized an older and more stable crust. However, details on the nature of crust required additional geophysical and geological data of high resolution in future studies.

Keywords *b*-value · Gravity anomaly · Continental crust · Oceanic crust · Northern Red Sea

✉ Ali K. Abdelfattah
aabdelfattah@ksu.edu.sa

¹ Department of Geology and Geophysics, King Saud University, Riyadh 11451, Kingdom of Saudi Arabia

² Department of Seismology, National Research Institute of Astronomy and Geophysics, Helwan, Cairo 11918, Egypt

³ Faculty of Sciences, Department of Geology, University of Tunis El Manar, Campus Universitaire, 2092 Tunis, Tunisia

1 Introduction

The Red Sea, which is actively transitioning to the seafloor spreading stage of ocean basin formation (Buck et al. 1988), is an example of a rift system on the continental shelf (Fig. 1). Although the Northern Red Sea (NRS) is influenced by the relative motion between the African and Arabian plates, due to its rigidity, the nascent rifting mechanism at the NRS is probably halting. Several authors are interested in studying the Red Sea rifting and the process of its opening; however, due to a lack of accurate data, especially for borehole data, numerous questions remain and the debate on this subject continues. In the absence of borehole data, the prevalence of the oceanic crust has proponents (LaBrecque and Zitellini

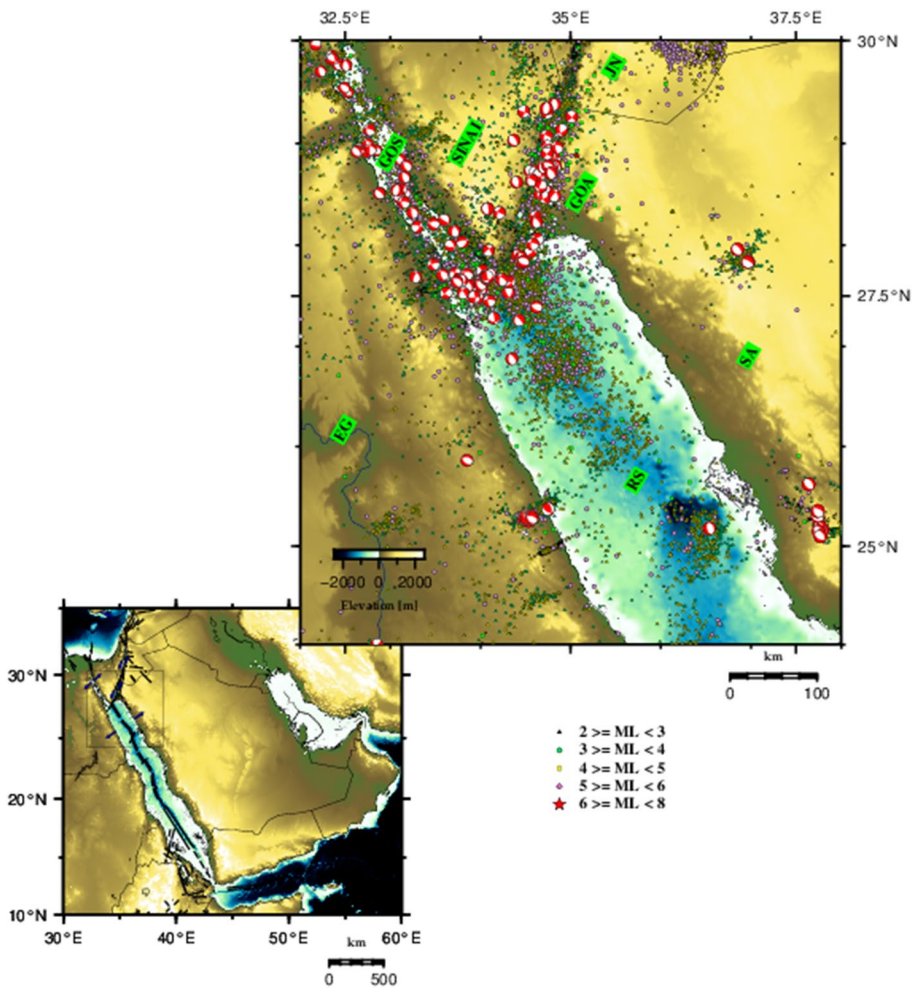


Fig. 1 Tectonics of the study region. The region is dominated by normal to strike-slip faulting mechanisms of earthquakes that occurred in the Gulf of Suez (GOS) and the Gulf of Aqaba (GOA), respectively. Extensional and shear deformations are associated with the relative tectonic movements between the Arabian and the African plates. (SA) Saudi Arabia, (EG) Egypt, (RS) Red Sea, and (JN) Jordan

1985; Girdler and Underwood 1985; Gaulier et al. 1988; Sultan et al. 1992; Dymant et al. 2013; Tapponnier et al. 2013) and opponents (Cochran 1983; Bonatti 1985; Cochran and Martinez 1988; Guennoc et al. 1988; Bosworth et al. 1993, 2005; Ghebreab 1998; Cochran 2005; Mitchell and Park 2014; Almalki et al. 2015, 2016). Stern and Johnson (2019) propose a volcanic rifted margin (VRM) model that consists of a continental breakup with an appearance of the marine basin. The NRS region is characterized by distinct deformation zones originating by tectonic or/and magmatic activities. Earthquake occurrences are direct evidence of geodynamic activities in the region. The distribution of earthquakes delineates that the seismic deformation zones occur along the axial rift of the Red Sea, Gulf of Suez, and the Gulf of Aqaba (Fig. 1), which may be caused by tectonic or/and magmatic activities. To investigate the tectonic implications and the prevalence of oceanic crust into the continental crust of the northernmost part of the NRS region, we present an analysis based on gravity, magnetic, and seismicity datasets.

GPS measurements and magnetic anomalies reveal seafloor spreading occurring in the southern Red Sea at a rate of ~18 mm/year, while the NRS demonstrates stretched continental crust and a slow-spreading rate of less than 10 mm/year (Chu and Gordon 1998; Cochran and Karner 2007; ArRajehi et al. 2010). However, the region is experiencing complex tectonic circumstances caused by the opening rift system in the Red Sea, shear deformation along the Gulf of Aqaba and Dead Sea fault, and the opening of the Gulf of Suez in addition to the active asthenosphere moving beneath the eastern and western flanks of the Red Sea. In the northernmost part of the NRS, three plate boundaries are demarcated and connected at an active triple junction; the axial rift of the NRS, the Gulf of Suez, and the Gulf of Aqaba. The passive rifting along the axial axis of the Red Sea initiated approximately 30 Ma, which in turn was followed by a period of active rifting (Daradich et al. 2003), causing stretching and thinning of the lithosphere due to an upwelling of magma along the axial rift of the Red Sea. Although the extensional stresses are dominant in the Gulf of Suez as inferred from the focal mechanism solutions of earthquakes (El-Nader and Hussein 2018), the northward continuation of continental rifting is speculated to have aborted or failed (Bosworth and Durocher 2017). In the Gulf of Aqaba, the extensional stress in the northernmost part of the NRS transitions into the shear type, and the structures of pull-apart basins are formed. This tectonic process causes an anticlockwise rotation of the Arabian plate of 6° at a rate of 1 cm/year relatively to the African plate (Garson and Krs 1976). Along the eastern and western flanks of the Red Sea coastline, a thermal uplift and a thinning of the overlying lithosphere lead to a wide distribution of Cenozoic basaltic fields named Harrats (Fig. 1). One model suggests that the origin of Cenozoic basaltic fields is caused by the magma migration from the Afar region to the north beneath the Arabian shield (Chang and Van der Lee 2011).

The integration of geophysical and seismological data provides insights into how geodynamic processes function within a region. Gravity and magnetic data are used to image heterogeneities and regional structures of either continental or oceanic crust. The spatial variation of b -values that are derived from the frequency–magnitude relationship is considered as a useful indicator to the state of stress, and therefore, it has been used to distinguish the tectonic origins of crustal structures. Several previous studies have discussed the correlation of b -values with other geophysical observations to interpret the tectonic implications of active tectonic regions (Wang 1988; Khan 2005; Khan and Chakraborty 2007; Sobiesiak et al. 2007; Kalyoncuoglu et al. 2011, 2013; Khan and Chakraborty 2007). Sobiesiak et al. (2007) used the spatial b -value distribution and isostatic residual gravity anomalies to identify the asperity structures in the north Chilean subduction zone. Global gravity and magnetic models compiled from satellites and airborne, marine, and terrestrial

measurements are sufficiently accurate and are considered a powerful tool that can reveal and provide details for regional tectonic processes, especially in marine areas (Sandwell et al. 2013, 2014). On the other hand, the b -value is a statistical parameter calculated from the frequency–magnitude relationship of Gutenberg and Richter (1941) and is mainly used to characterize seismic activity in terms of a wide range of magnitude scales based on tectonic environments, stress heterogeneities, and anisotropic mediums. A wide spatial distribution of b -values, from low to high, is related to high and low stress accumulations reflecting structural heterogeneities due to the presence of diversely oriented cracks. A high b -value characterizes the seismicity of small magnitude events, while a low b -value characterizes the ratio number of larger earthquakes to smaller ones (Wyss and Stefansson 2006). In magmatic activity zones, the seismicity is characterized by high b -values (Sánchez et al. 2004), thereby implying low effective stress regimes that might link to high pore pressures (Wyss 1973) or geothermal gradients (Warren and Latham 1970).

2 Tectonic Settings

The study region represents a natural laboratory that can be used to understand various processes during a newly born continental plate boundary, including early continental rifting, the formation of ocean basins, and continental transformations due to complex tectonic movements represented by active convergence and divergence movements occurring at the Arabian–Turkish and the African–Arabian plate boundaries, respectively (Fig. 1). Owing to the active tectonic breakup of the Arabian plate from the African plate, the Red Sea rift was generated during the Miocene with three distinct tectonic units: the NRS rift, the Gulf of Suez rift, and the Gulf of Aqaba–Dead Sea transform fault. These structures are bounded by continental flanks that are called the Arabian–Nubian shield; these flanks are comprised of Precambrian magmatic and metamorphic rocks due to the Pan-African orogeny (Bentor 1985; Stern 1994; Stein and Goldstein 1996; Stern and Johnson 2010). The Cenozoic tectonic regime in the Arabian–Nubian shield is mainly controlled by an active asthenosphere that causes thinning, uplifting, extension, and rifting of the lithosphere. Consequently, the shield is enriched by geothermal activities associated with seismic and magmatic activities on both sides of the NRS. Two distinct zones are widely known: the Abu Dabbab seismic dislocation zone in Egypt and Al-Ays seismic dislocation zone that is associated with magmatic intrusions in the Arabian shield, western Saudi Arabia.

From a tectonic point of view, the geodynamic extension is dominant and produces normal faults in the NRS and the Gulf of Suez, while the oblique extension creates dip-slip and sinistral strike-slip faults along the Aqaba–Dead Sea fault. The evaluation of geodynamic processes in the NRS suggests several magma-poor to magma-rich scenarios. Bosworth (2015) suggests a rift-to-drift transition of the magma-poor hyperextended basin. On the other hand, several studies have proposed a triple junction that connects the NRS rift, the Gulf of Suez, and the Gulf of Aqaba, which has developed since the early middle Miocene (Freund et al. 1970; Joffe and Garfunkel 1987; Cochran 2005). Ehrhardt and Hübscher (2015) explored the axial zone of the NRS, which is considered to be volcanically and tectonically active. Different tectonic interpretations presume that the rifting extends from the Red Sea into the Suez Rift in the middle Miocene and becomes an aborted continental rift in the Precambrian shield south of Sinai. The active Gulf of Aqaba was initiated by a breakup of the Arabian plate from the Sinai subplate, and this breakup has remained active since the Middle Miocene orogeny (Mart and Horowitz 1981; Mart and Rabinowitz 1986).

The local magnetic occurrences that outcrop in the NRS suggest a small number of volcanoes that represent the proximity of basaltic magma chambers (Guenoc et al. 1988). The NRS and the southern part of the Gulf of Suez revealed an extensional stress regime, while the shear stress regime controlled the tectonic deformation in the Gulf of Aqaba–Dead Sea fault zone (Abdel-Fattah et al. 2016). Notable earthquakes occurred in the NRS in 1969 and 2001, and in the Gulf of Aqaba in 1993 and 1995 (Ben-Menahem and Aboodi 1971; Badawy and Abdel-Fattah 2006). After increasing the number of seismic measurement stations in Egypt and Saudi Arabia, earthquakes have been recently observed inside several dislocation zones inside the Arabian–Nubian shield. A focal mechanism is commonly used to deduce the tectonic implications by investigating faulting styles, and stress accumulations in the northernmost part of the NRS region are shown in Fig. 1.

3 Data Analysis and Results

To study the spatial distribution of b -values, we collected available earthquake catalogues from the International Seismological Center (ISC), the Egyptian Seismographic Network (ESN), and the Saudi Seismographic Network (SSN). The collected catalogues were filtered by removing artifacts and duplicate events. The compiled catalogue covers the region between 23.50° N– 32.59° N and 30.98° E– 40.57° E and the period spans from 1900 to 2019. We collected 124 focal mechanism solutions from different resources (Global Centroid Moment Catalog (GCMC), International Seismological Center (ISC), and several publications) for earthquakes that occurred between 1969 and 2016. Figure 2 shows the earthquake frequency with depth histograms for the Gulf of Aqaba, Gulf of Suez, and clusters in the northern Red Sea region. Since the earthquake catalogue recorded by different networks in the region has different magnitude scales, it is important to unify the magnitude scale. For this purpose, we used a series of empirical Eqs. (1–5) to unify all magnitudes to the moment magnitude scale:

$$M_w = \exp(2.133 + 0.063M_s) - 6.205, \quad (1)$$

$$M_w = \exp(0.719 + 0.212m_B) - 0.737, \quad (2)$$

$$M_w = 0.546 * M_L + 1.2849, \quad (3)$$

$$M_L = 0.8062M_D + 0.6049, \quad (4)$$

$$M_D = 1.1721M_m - 0.4889. \quad (5)$$

Equations 1 and 2 are taken from Lolli et al. (2014). Figure 3 shows the empirical relationships developed to calculate the moment magnitude.

3.1 Mapping of b -values

The b -value is a statistical parameter that provides implications on seismotectonic settings and potential seismic hazards in a given region. It can be calculated using the frequency–magnitude relationship (Gutenberg and Richter 1941):

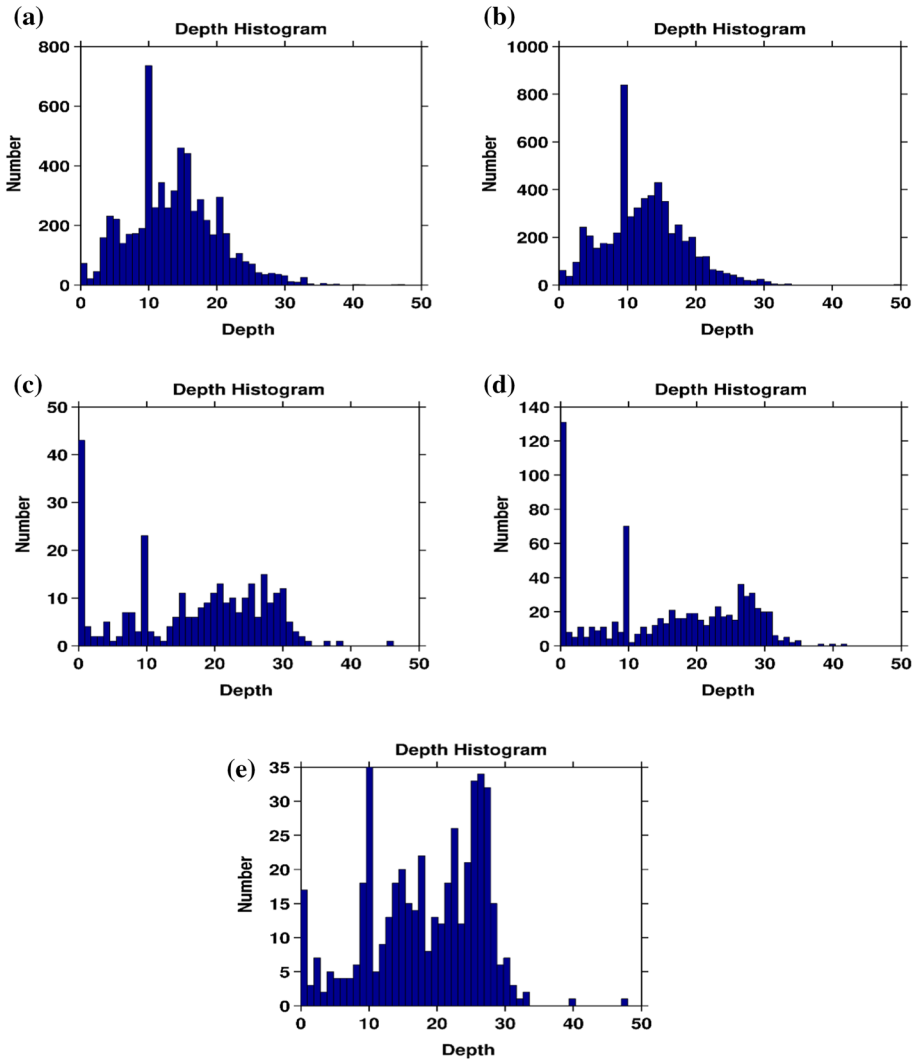


Fig. 2 Histogram of earthquakes’ depth distribution in the Gulf of Suez (a), Gulf of Aqaba (b), and selected zones in the northern Red Sea (c–e) region

$$\log_{10} N(M) = a + bM, \tag{6}$$

where $N(M)$ is the cumulative number of earthquakes in the magnitude range $\geq M$. The coefficient “ a ” represents the seismic activity and varies from 2 to 8 depending on the size of the deformation area, time span, number of earthquakes, and magnitude ranges. The b -value mainly depends on the nature of tectonic settings, crustal heterogeneity, pore fluids pressure, and stress state (Schorlemmer et al. 2005; Khan and Chakraborty 2007; Mousavi 2017a, b). We used the maximum likelihood technique of Aki (1965) to quantify the b -value using the following equation:

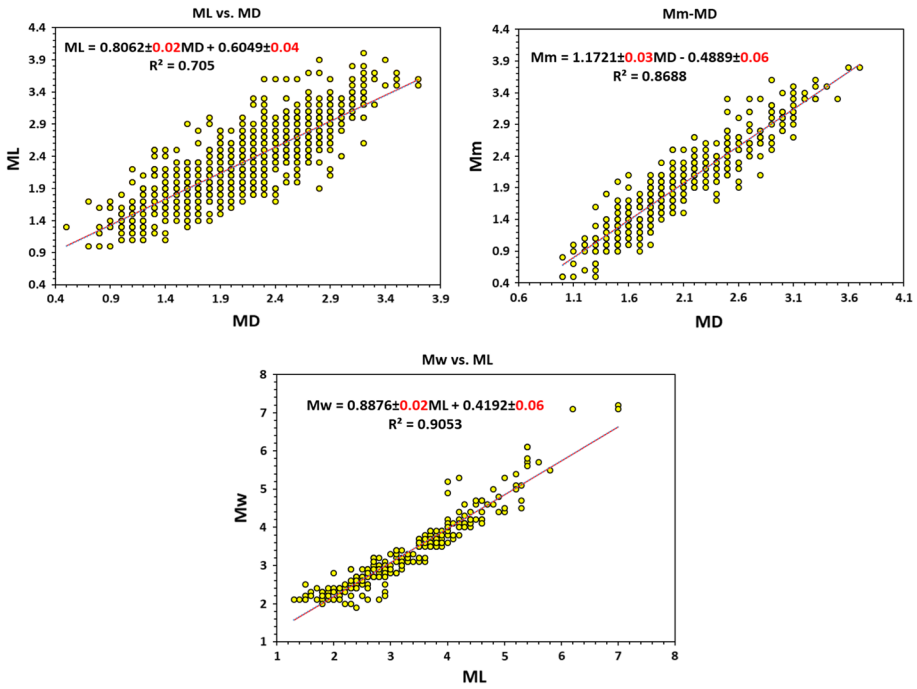


Fig. 3 Empirical linear relationships developed to convert the magnitude into different magnitude scales: (M_w) moment magnitude, (M_L) local magnitude, (M_D) duration magnitude and (M_m) mantle magnitude

$$\hat{b} = \frac{\log e}{\bar{m} - \left(M_{\min} - \frac{\Delta m}{2} \right)} \tag{7}$$

where m is the mean magnitude, \hat{b} is the estimate of b , M_{\min} is the magnitude cutoff above which the catalogue is complete, and $\Delta m/2$ is a correction for the finite binning width (Δm) of the original catalogue. To map the spatial distribution of the b -values, the ZMAP software of Wiemer and Zuñiga (1994) was used. The study area was discretized into square grids. Each grid had a dimension of $0.2^\circ \times 0.2^\circ$ and overlapped with neighboring grids by 0.1° in both latitude and longitude to maintain the continuity of the data points. The b -value was calculated at each grid node of 0.1° along both latitude and longitude. The weighted least-squares method was applied to a minimum number of $N_{\min} = 100$ events. The temporal variation of M_c (magnitude completeness) was negatively correlated with the number of seismographs and the development of analysis methods. To reduce errors in the b -value estimation, we investigated the spatiotemporal variations in M_c (Figs. 4, 5). An abrupt change was observed after 1995, as shown in Fig. 5a, b, which may be attributed to an increase in the number of seismic stations in the region. Consequently, the estimation demonstrated a uniform fluctuation rate. Shi and Bolt (1982) proposed the evaluation of uncertainties in the spatial distribution of b -values as

$$\hat{\sigma}_{b^*}^{(SB)} = 2.30 \hat{b}^{*2} \sqrt{\frac{\sum_{i=1}^N (M_i - \hat{\mu})^2}{N(N-1)}}, \tag{8}$$

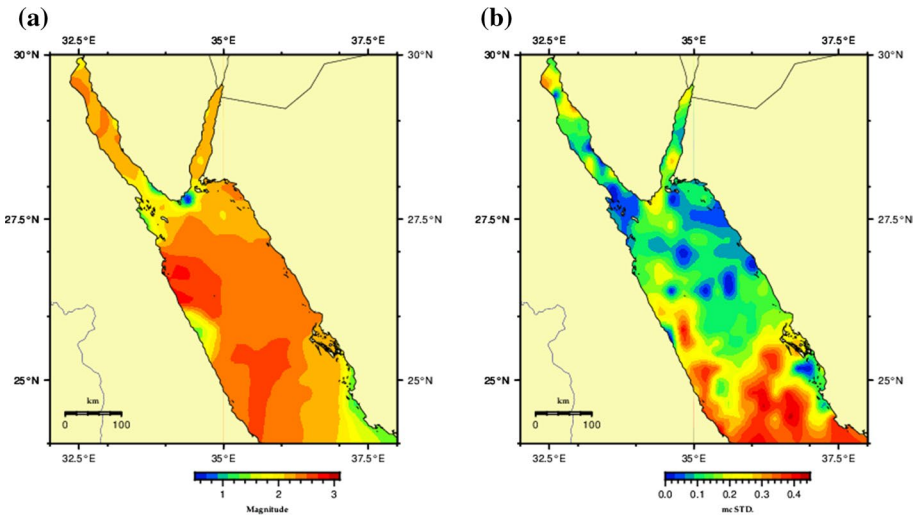


Fig. 4 Spatial distribution of magnitude completeness (a) and standard deviation of magnitude completeness (b) in the study area that discretized into square grids of a dimension of $0.2^\circ \times 0.2^\circ$ and overlapped a grid node of 0.1° along both latitude and longitude

where N is the number of earthquakes. The bootstrap approach was used to assess the errors in b -values (Chernick 1999). The interpolated map of the b -value spatial distributions is shown in Fig. 6a. It is evident from the figure that b -values vary between 0.54 and 1.08. The reliability of b -value calculations was evaluated by the respective error estimations as shown in Fig. 6b.

3.2 Seismic Moment

The seismic moment release can be used to describe a stress release (Aki 1966). To elucidate stress accumulation, the seismic moment (M_o) was calculated from the moment magnitude (M_w) using the relationship of Kanamori and Brodsky (2001)

$$\log_{10} (M_o) = 1.5 M_w + 9.1 \quad (9)$$

To map the spatial variation of seismic moment releases, as shown in Fig. 7, the estimated seismic moments were summed within $0.2^\circ \times 0.2^\circ$ square grids and overlapped with neighboring grids by 0.1° in both latitude and longitude to preserve the continuity of the data points.

3.3 Gravity and Magnetic Data Analysis

We used the high-resolution ($2' \times 2'$) global grid model of Earth gravity anomalies known as WGM2012 (Bonvalot et al. 2012), which is computed at the global scale in spherical geometry by the Bureau Gravimétrique International (BGI) in collaboration with other international organizations. These anomalies were derived from the Earth's global gravity model of EGM2008 (Pavlis et al. 2012) and the Earth's topography–bathymetry ETOPO1

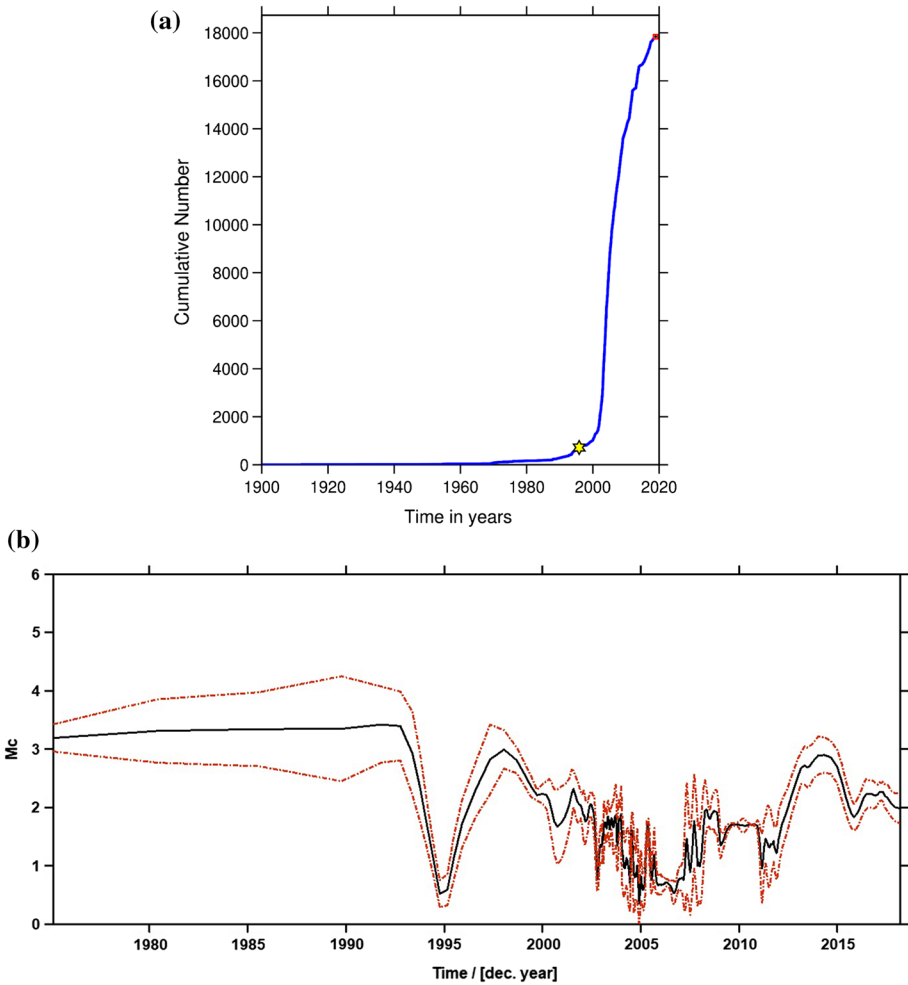


Fig. 5 **a** Time series curve for the compiled earthquake catalogue used in the analysis, showing cumulative number of earthquakes as a function of time, **b** temporal variation of the estimated magnitude of completeness (solid line) and its standard deviations (dashed lines) applying maximum curvature method (MAXC) (Wiemer and Wyss 2000)

data. EGM2008 and ETOPO1 were used to compute gravity anomalies (Balmino et al. 2011; Bonvalot et al. 2012). Such global anomalies are highly useful in revealing regional crustal structures. Figure 8 shows the free-air anomaly maps of the study area.

The free-air anomaly map shows negative anomalies in the Gulf of Sinai and Gulf of Aqaba, implying that the lack or deficiency of mass below sea level is not completely compensated by a thinning of the crust. However, in the NRS, the map (Fig. 8) shows positive and negative anomalies of high frequencies trending in different directions. These anomalies are not related to the heterogeneities of the regional lithospheric structure, rather than that at shallow depth. The overall free-air anomalies in the Red Sea imply a weak behavior (low elasticity) of the lithosphere caused by a thinning of crust in this area. As the free-air anomalies reflect the deficiency of mass below sea level and density contrasts

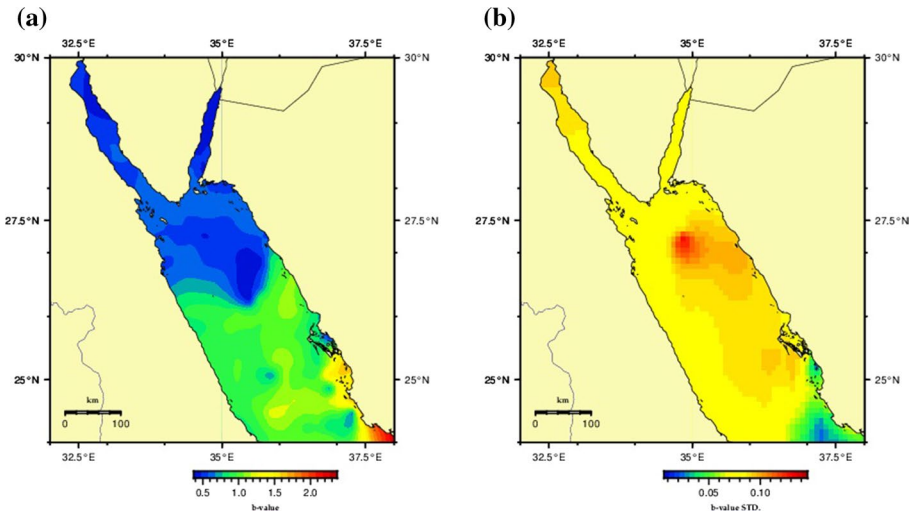


Fig. 6 Spatial distribution of b -values (a) and standard deviation of b -values (b). The study area was discretized into square grids of a dimension of $0.2^\circ \times 0.2^\circ$ and overlapped by 0.1° to maintain the continuity of the data points. The b -value was calculated at each grid node of 0.1° along both latitude and longitude. The uncertainties in the spatial distribution of b -values were estimated based on the empirical relation proposed by Shi and Bolt (1982)

within the lithosphere, including the Moho discontinuity, we calculated Bouguer anomalies. Bouguer anomalies (Fig. 9a) were obtained after removing the effect of deficiency of mass below sea level from the observed free-air anomalies; this effect was represented by the water layer using 2.70 and 1.035 g/cm^3 as the density of crust and water, respectively. The obtained Bouguer anomalies show long and short wavelengths due to density contrasts in the subsurface, including the real root of the crust that compensates for a part of the total deficiency of mass below sea level. To better observe the effect of the crustal thickness variation and large-scale structures expressed by long-wavelength anomalies, we have attenuated short wavelength by upward continuation (Fig. 9b). The upward Bouguer anomaly map shows prominent negative anomalies in the Gulf of Aqaba and Gulf of Suez due to root of the crust, thereby implying that the crust in this area is not thin enough to compensate for the lack of mass represented by water; thus, the crust in these regions is still rigid. Conversely, in the Red Sea, in addition to high-frequency anomalies related to shallow depth heterogeneities, a regional positive gravity trend occurs along the axial rift of the Red Sea and the anomaly becomes negative toward the western and eastern edges. This observed anomaly is due to the thinning of the crust along the trough of the Red Sea. As the crust of the Red Sea is thin enough to compensate for the lack of mass represented by the water, the crust is considered weak and not rigid.

To comprehensively constrain the effect of density contrasts within the crust, we removed the crustal root effect based on the Airy model from the observed Bouguer anomaly by assuming a density of 2.70 and 3.30 g/cm^3 for the crust and the mantle, respectively. The obtained values are determined by isostatic anomalies (Fig. 10a) that should represent only the response of the density heterogeneities within the crust. This would be true in the Red Sea as the crust is effectively thinned. In the Red Sea, even with the lack of material and the mass deficiency represented by the seawater, we do not observe a specific long-wavelength isostatic anomaly (Fig. 10a). The isostatic anomaly map shows a number

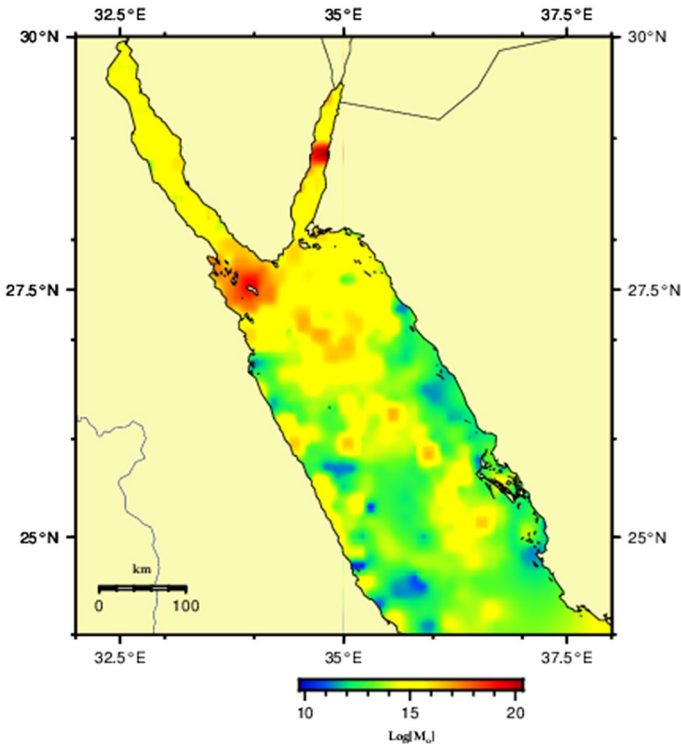


Fig. 7 Spatial variation of the cumulative seismic moment releases in the study region that discretized into grid cells of a dimension of $0.2^{\circ} \times 0.2^{\circ}$ overlapped by 0.1° grid nodes along the latitude and longitude to preserve the continuity of the data points

of short-wavelength anomalies with low positive or negative amplitudes trending in the NW–SE and NE–SW directions that are parallel and conjugate, respectively, to the Red Sea axial rift. These short-wavelength anomalies are due to density heterogeneities at shallow depth (dikes or faults). In order to enhance these short-wavelength anomalies, we calculated the vertical gradient. This process makes the gradient of shallow depth sources' anomalies much stronger than those of deep sources. Such a process based on gradient of gravity anomalies has been applied by Pamukçu (2016) to locate boundaries in eastern Mediterranean region. Shallow sources in NRS crust are better observed on the vertical gradient of the isostatic anomalies (Fig. 10b).

Magnetic anomalies are widely used to constrain subsurface structures and crust composition. We used Global magnetic anomaly EMAG2 (Meyer et al. 2017), which consists of a merged grid compiled from all available magnetic measurements and represents the total magnetic anomalies at 4 km above the geoid in a 2-arc-minute resolution. Figure 11 shows the magnetic anomalies of the study area. There is evidence of positive and negative anomalies lengthened in the NW–SE and NE–SW directions. These anomalies are related to magnetic heterogeneities due to dikes or mega faults within the crust. Trends parallel to the Red Sea may be related to the main rifting and they are scattered by NE–SW trends in the Arabian shield and E–W trends in Sinai, and they should be related to mega faults separating compartments with different magnetic behaviors.

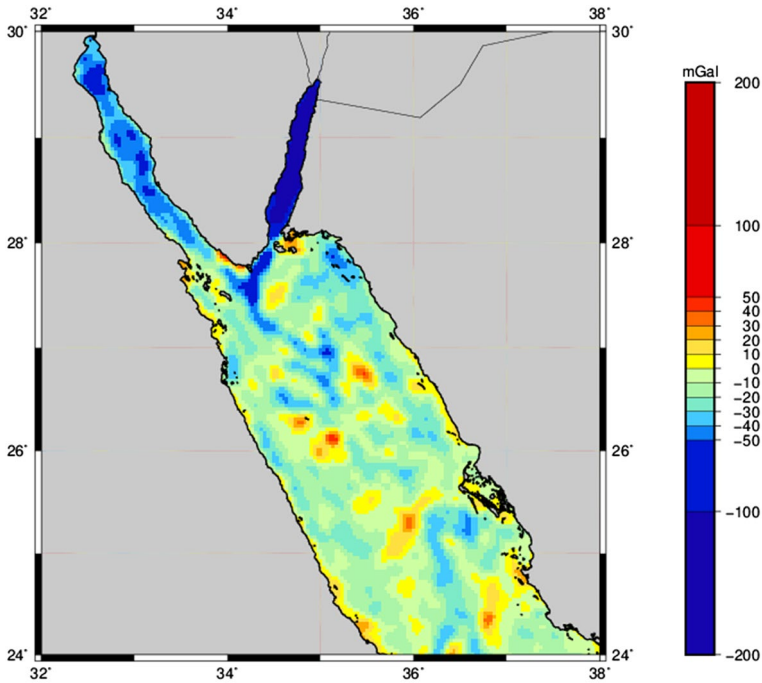


Fig. 8 Free-air anomaly map of the NRS region derived from WGM2012. The Gulfs of Aqaba and Suez show negative anomalies, whereas NRS shows short wavelengths with positive and negative anomalies containing low amplitudes trending in different directions

4 Discussion

The weak continental crust characterizes the northernmost portion of the Red Sea, while the crust of the southern part is categorized as oceanic nature except for the edges of coastlines (Mitchell and Stewart 2018). The shear deformation in the Levant fault zone is presumably responsible for this disparity (Gaulier et al. 1988). The integration of geophysical and seismological data provides general insights into the tectonic process acting in the northernmost part of the Red Sea region. Results of deep seismic soundings in the NRS (Rihm et al. 1991) represent a thin continental crust beneath the eastern and western flanks (Al-Amri 1995). The results of velocity tomographies of El Khrepy et al. (2016a, b) strongly suggest the occurrence of a heterogeneous continental crust beneath the Gulf of Aqaba and the Gulf of Suez. Moreover, the evidence of high seismicity (Fig. 1), high-density crustal layers just beneath evaporites (El-Bohoty et al. 2012), low seismic velocity gradients (Gaulier et al. 1988), and Precambrian shield rocks (Bosworth et al. 1993; Almalki et al. 2015) support that the NRS is covered with a thin continental crust, with a few isolated sites emplaced by basaltic injection (Cochran 2005; Mitchell and Park 2014; Mitchell and Stewart 2018). The lack of linear magnetic anomalies suggests that the Miocene evaporites were deposited on an attenuated continental lithosphere and motivated higher temperatures. This is a potential indication of an early stage of a tectonic regime associated with continental separation, rifting, and crustal thinning prior to the seafloor spreading and the accretion of oceanic crust (Mart and Hall 1984). The region is characterized

by a crust to upper mantle heterogeneities associated with localization of stress accumulations due to the coupling of tectonic and magmatic processes. These crustal heterogeneities can be identified by modern geophysical tools like tomography and gravity, although they cannot account for the stress heterogeneities. As mentioned above, gravity analysis shows evidence of crustal thinning toward the trough of the Red Sea and heterogeneities due to magmatic intrusions. One of the distinct indicators to distinguish the heterogeneity of the crust and stress is the b -value that can be computed using the frequency–magnitude relationship. The variation in b -values is ascribed to the material heterogeneity (Mogi 1963) and the stress state (Scholz 1968; Urbancic et al. 1992; Schorlemmer et al. 2004, 2005) or effective stress (Wyss 1973), and the thermal gradient may increase b -values (Warren and Latham 1970). Mogi (1967) primarily considered the nature of rock mechanics, while Scholz (1968) speculated that the b -value is influenced by the stress behavior rather than by the heterogeneity of the rock's material. Scholz (1968) and Wyss (1973) observed that low b -values correspond to periods of increasing shear stress or effective stress. Increased rock mass heterogeneity or crack density results in high b -values (Mogi 1967), while resistant blocks (asperities) embedded in rocks decrease the b -values.

Based on the free-air anomaly map, there is evidence that the deficiency of mass below sea level is not completely compensated by a thinning of crust in the Gulf of Aqaba and Sinai; conversely, the overall free-air anomalies in the NRS correlate with a weak behavior (low elasticity) of the lithosphere that occurred through a thinning of crust in this area. Bouguer anomalies that reflect only density contrasts in the subsurface, including the real root of the crust, are prominently negative in the Gulf of Aqaba and Gulf of Suez; these negative anomalies imply that the crust in these areas is not thin enough to compensate for the lack of mass represented by water, and we may deduce that the crust in these regions is still thick and rigid. As the amplitudes of negative Bouguer and isostatic anomalies are lower in the Gulf of Suez than in the Gulf of Aqaba, we may deduce that the crust is thinner and weaker in the Gulf of Suez. Conversely, in the Red Sea, we do not observe a specific long-wavelength negative Bouguer anomaly. There is evidence of several short-wavelength anomalies with low positive or negative amplitudes that trend mainly along the NW–SE direction, which is parallel to the Red Sea rifting, and the NE–SW direction, which is perpendicular to the Red Sea rifting. These anomalies are due to density heterogeneities within shallow depths of the crust. In addition to short-wavelength anomalies related to shallow depth heterogeneities, we observe a regional Bouguer positive anomaly trend along the axial rift of the Red Sea, and the anomaly becomes negative toward the western and eastern margins. This observed anomaly is due to the thinning of the crust from the shield toward the trough of the Red Sea. As the crust of the Red Sea is thin enough to compensate for the lack of mass represented by the water, the crust is considered weak and not rigid. The isostatic anomaly map is only supposed to represent the effect of density heterogeneities within the crust, and it does not show a specific long-wavelength isostatic anomaly in the NRS. The map only shows several short-wavelength anomalies with low positive or negative amplitude trending in different directions. This observation confirms that the crust in the NRS, due to its weakness, is sufficiently thinned to compensate for the deficiency of mass represented by a water layer. The positive Bouguer anomalies are related to thinner and weaker crust which leads to higher stress accumulation. This behavior is not observed in the Gulf of Aqaba and the Gulf of Suez, indicating a prominent negative anomaly associated with a relatively thicker crustal root that causes lower stress accumulation.

The magnetic anomaly map shows evidence of positive and negative anomalies lengthened in NW–SE and NE–SW directions as observed in the Red Sea area and Arabian shield. These anomalies are related to magnetic heterogeneities caused by dikes or mega

Fig. 9 **a** Bouguer anomaly map of the NRS region obtained after removing the effect of deficiency of mass below sea level from the observed free-air anomalies, represented by the water layer using 2.70 and 1.035 g/cm³ as the density of crust and water, respectively. The Gulfs of Aqaba and Suez show negative anomalies, whereas NRS shows a regional positive gravity trend along the axial rift of the Red Sea, and the anomaly becomes negative toward the western and eastern edges. **b** Upward continuation of the Bouguer anomaly map of the NRS region. Short-wavelength anomalies are attenuated. Contour interval: 20 mGal. Smooth increasing of Bouguer anomaly values due to thinning of the crust toward the Red Sea axial rift

faults within the crust. Such magnetic trends correlate with the gravity trends described above and are supposed to be related to density heterogeneities within the crust. NW–SE gravity and magnetic trends that are parallel to the Red Sea should be related to the main rifting. These structures are scattered by NE–SW trends observed in the Red Sea and Arabian shield. These trends should be related to mega faults separating compartments with different magnetic behaviors.

Gravity and magnetic analyses show that the NRS is characterized by a weak crust with evidence of thinning toward the trough of the Red Sea, whereas the crust remains thick and relatively rigid in the Gulfs of Aqaba and Suez. This result confirms the study of Cochran (2005), where he suggests a thinning of the continental crust of the NRS up to 5 km based on the integration of marine geophysical data, including seismic reflection. This author suggests also nucleation of oceanic spreading in the main trough of the NRS. This thinning of the continental crust is confirmed by Saleh et al. (2013) based on the mapping of the Curie point depth and heat flow. These authors show evidence of an increase in the heat flow of up to 250 mW/m² and a decrease in the Curie depth of up to 5 km. Figure 12 shows the spatial distribution of the heat flow data as combined from the global oceanic heat flow measurements in Lucazeau (2019), the global area-weighted heat flow model in Davies (2013), and aeromagnetic data in Saleh et al. (2013). Based on the spatial resolution and the accuracy of the data, priority is given to the global database in Lucazeau (2019) at the overlapping areas with other data sources. Notably, the interpolated map shows a low resolution due to the deficiency in the heat flow data. However, the high heat flow patterns distribute approximately along the central area of the NRS region. Low heat values dominate within the regions representing the Gulf of Aqaba, the Gulf of Suez, and the coastlines of the NRS. The gravity and magnetic anomalies of short wavelengths indicate crustal heterogeneities due to mega faults, intruded dikes and volcanic activity associated with the trends that are parallel and conjugate to the Red Sea axial rifting.

The spatial variations in *b*-values are factorized to the material heterogeneity, stress accumulation, perturbation in the pore fluid pressure, and thermal activities (Edrik et al. 2012; Görgün 2013). For regions of different tectonic environments, the *b*-value ranges from 0.5 to 1.5 with a wide range of magnitude scales (Wiemer et al. 1998). In the active volcanic regions where seismicity is triggered by magmatic activities, the *b*-value is anticipated within the range of 1.5–3.0 (McNutt 2005). Moreover, the regions of high-density fractures and stress heterogeneities are characterized by *b*-values ranging between 1.0 and 2.5 (Bridges and Gao 2006). The pattern of the *b*-values (Fig. 6a) shows wide variations in the *b*-value from 0.4 to 2.5. The variations in *b* value patterns characterize alternating areas of low to high *b*-values and are likely caused by the heterogeneity of either the stress field or material properties. The Gulf of Aqaba and the Gulf of Suez regions exhibit low *b* values, while the rest of the NRS regions display alternating low to high *b*-values. Low *b* values that are obtained in the Gulf of Aqaba, the Gulf of Suez, and the northmost part of the NRS are consistent with the *b*-values estimated by El-Isa and Shanti (1989) and Al-Amri (1995). The local structures of hardness materials in the south of Sinai presumably

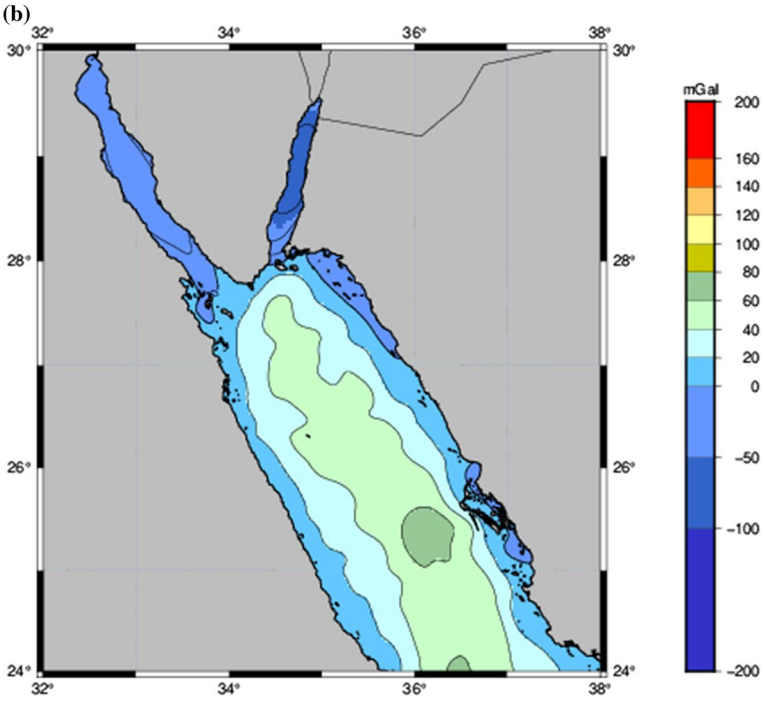
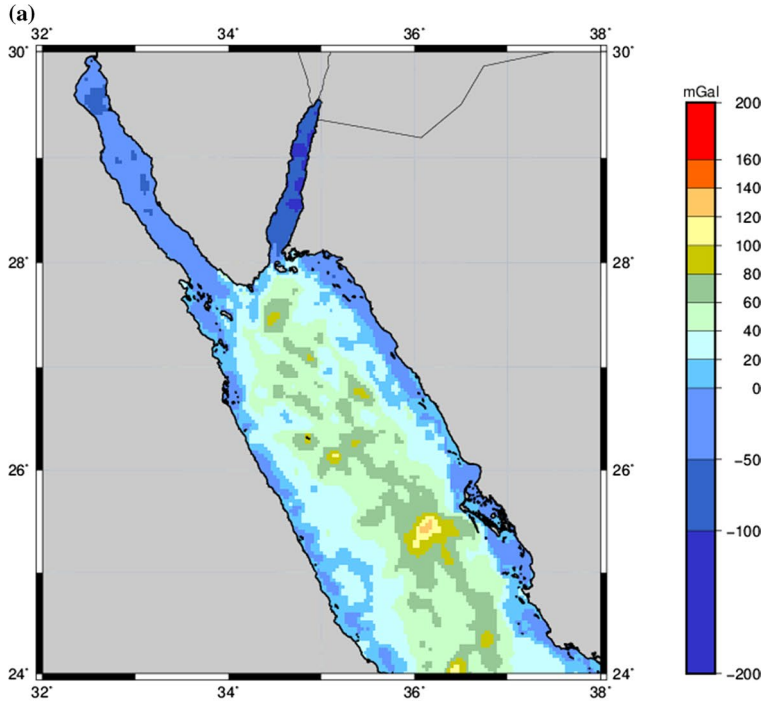
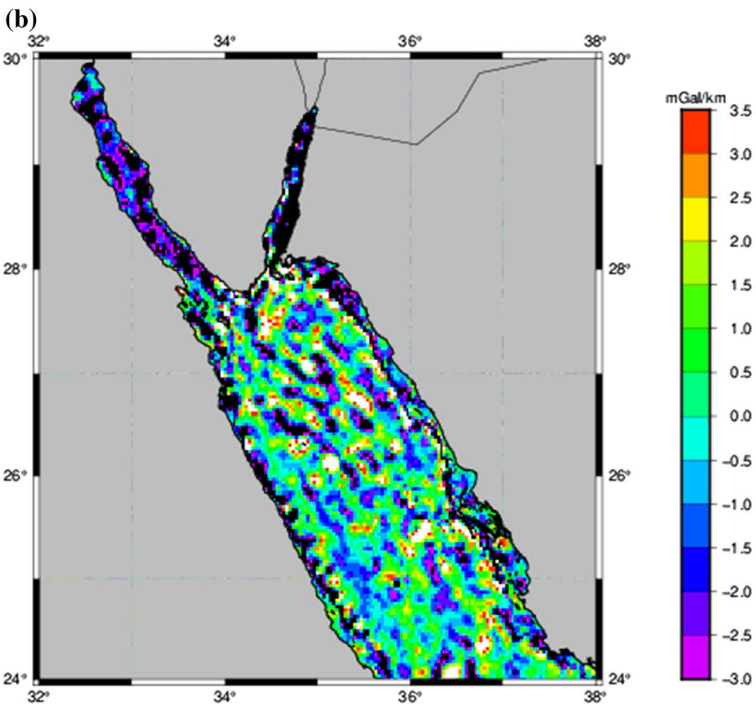
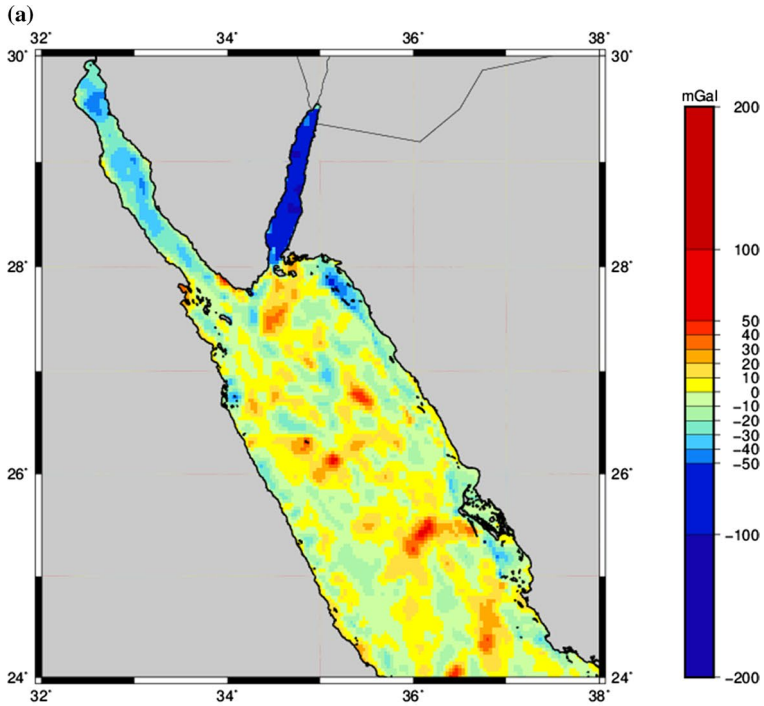


Fig. 10 **a** Isostatic anomaly map of NRS region obtained by removing the effect of crustal root based on the Airy model from the Bouguer anomalies, assuming a density 2.70 g/cc and 3.30 g/cc for the crust and the mantle, respectively. The Gulfs of Aqaba and Suez show negative anomalies, implying that the crust in these areas is not thin enough to compensate for the deficiency of mass represented by water at the surface, whereas the NRS shows a number of short-wavelength anomalies with low positive or negative amplitudes trending in NW–SE and NE–SW directions that are parallel and conjugate, respectively, to the Red Sea axial rift. **b** The vertical gradient of the isostatic anomaly map of NRS region. Short-wavelength anomalies trending in NW–SE and NE–SW directions that are parallel and conjugate, respectively, to the Red Sea axial rift are enhanced

impede the Red Sea rift toward the north (Gaulier et al. 1988). Seismic tomography studies of El Khrepy et al. (2016a) reveal that no signs of the transition of oceanic crust into the Gulf of Aqaba have occurred, implying that the rift is standing at the triple junction due to local structures of high rigidity. Alternatively, the breakup of continental rupture in the NRS is presumed to occur in a relatively non-volcanic mode as reported from different geophysical and geological aspects (Ligi et al. 2018). Notably, variations of seismicity rates along the Gulf of Suez imply that the active stress regime is spatially non-uniform (Bosworth and Durocher 2017). The rate of crustal deformation in the Gulf of Aqaba is larger than those in the rest of the NRS region. GPS measurements revealed a northward movement of the Sinai micro-plate with respect to Africa at a rate of ~ 1.5 mm/year and a rifting rate of ~ 0.5 mm/year in the Gulf of Suez (Wdowinski et al. 2004; Gomez et al. 2007). The Gulf of Aqaba experienced a shear deformation aligned along a strike-slip fault at a rate of 4.4 ± 0.3 mm/year (Mahmoud et al. 2005). The moment tensor summations revealed a crustal deformation rate of 0.008 mm/year in the Gulf of Suez (El-Nader and Hussein 2018) and a rate of 0.32 ± 0.05 mm/year in the Gulf of Aqaba (Almadani 2020, personal communication). The relatively faster divergence rate, to the south, corresponds to an increase in *b*-values and cumulative moment releases, indicating a directly proportional relationship between the divergence rate and *b*-values within the study region.

Comparisons of the spatial distribution of *b*-values, cumulative seismic moment releases, and Bouguer gravity anomalies indicate interesting implications for detailing the crustal and stress heterogeneities. Khan and Chakraborty (2007), Maden and Öztürk (2015), and Pamukçu (2016) correlate the gravity data with the heat flow measurements and the spatial mapping of *b*-value in the Shillong Plateau, eastern Anatolian fault, and Eastern Mediterranean region, respectively. In Shillong Plateau area, Khan and Chakraborty (2007) attributed the observations of positive Bouguer anomalies and low *b*-values to a thinner crustal root and higher stress accumulation, whereas negative Bouguer anomalies and intermediate to high *b*-values are attributed to a thicker crustal root and lower concentration of stress. In the eastern Anatolian fault, the results were interpreted that the crustal root is comparatively thicker in areas characterized by the negative gravity anomalies, low *b*-values and lower stress concentration (Maden and Öztürk 2015). On the contrary, the authors attributed the correlation between positive gravity anomalies and high *b*-values to weaker and thinner crust consistent with higher concentration of stress. The correlation between Bouguer anomalies and *b*-values remains not clear. The relationship between them could be proportional or inverse proportional. However, in general, gravity boundaries due to structural transition associated with long-wavelength Bouguer anomalies and *b*-value variations are consistent. The results of Pamukçu (2016) shows that Bouguer boundaries determined in Crete and Rhodes islands in Eastern Mediterranean region are parallel to *b*-value variation. On the relationship between *b*-values and stress, an inverse proportional relationship is observed between the stress and the *b*-value for different regions (Wiemer and Katsumata 1999; Lei 2003; Schorlemmer et al. 2005; Maden



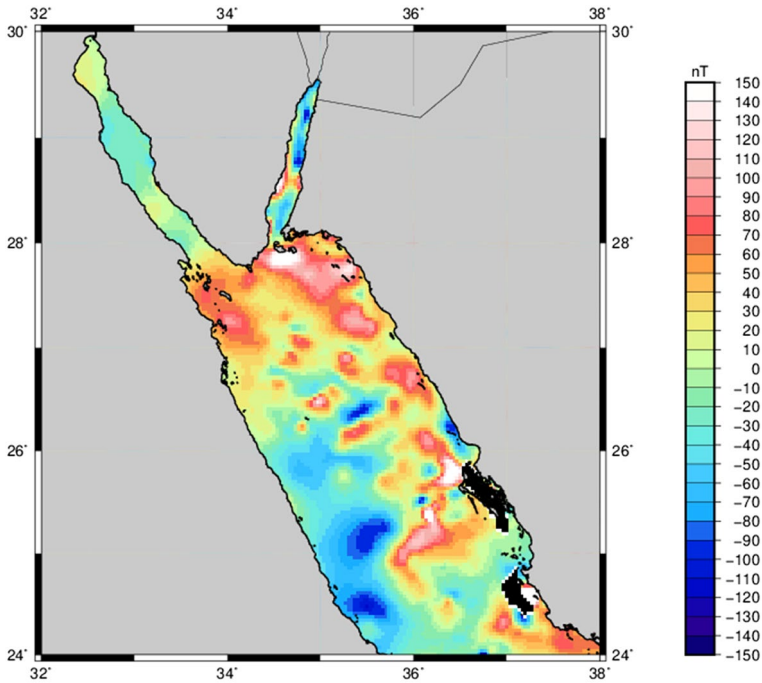


Fig. 11 Total magnetic anomalies at 4 km above the geoid of the NRS region derived from the Global magnetic anomaly EMAG2 (Meyer et al. 2017). A portion of positive and negative anomalies lengthened in the NW–SE and NE–SW directions

and Öztürk 2015; Mousavi 2017a). However, the b -value is not widely accepted to be used as a typical indicator to the stress assessment, but it can be used for some proxies. Therefore, it is crucial to integrate different geophysical data to understand the state of the stress accumulation. Following the interpretation method of Khan and Chakraborty (2007), we combined results from the Bouguer gravity anomaly, heat flow, and b -value maps. Except for the locations that corresponded to two large earthquakes with moment magnitudes of 6.3 and 7.3 occurred in the Gulf of Aqaba in 1993 and 1995, respectively, and the 1969 earthquake of moment magnitude 6.2 that occurred in the Gulf of Suez. Furthermore, it is noteworthy that the earthquakes occurred in the Gulf of Aqaba and the Gulf of Suez are characterized by low stress-drop values (Abdelfattah et al. 2019). In general, except for the areas of large-sized earthquakes that are characterized by high stress accumulation, the negative gravity anomaly values and lower heat flow that located in the Gulf of Aqaba and the Gulf of Suez regions are corresponding to low b -values and low stress accumulation, implying an old comparatively thicker crust. Conversely, the rest of the NRS region is characterized by the positive gravity anomalies with relatively high heat flow, and high stress accumulation and high b -values are associated with relatively weakened or young crust, thus implying magma upwelling or low-velocity zones.

The tectonic elements of the NRS region (Fig. 1) show an active deformation associated with normal to strike-slip faulting mechanisms that are dominant in the Gulf of Suez and the Gulf of Aqaba, respectively. The tectonic movement of the Arabian plate toward the north with respect to the Sinai subplate, which accommodated by the accumulation of shear stress,

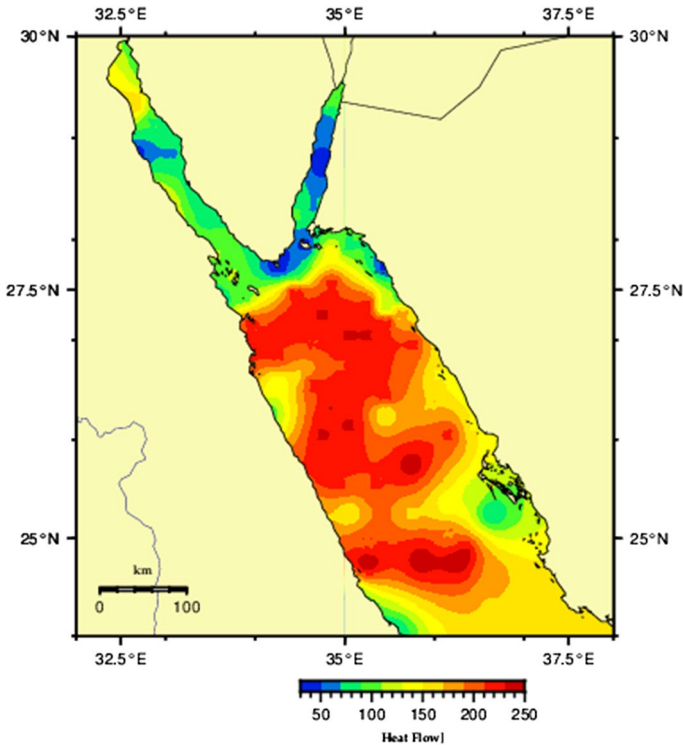


Fig. 12 Spatial distribution of the heat flow data combined from the global oceanic heat flow measurements in Lucazeau (2019), the global area-weighted heat flow model in Davies (2013), and from aeromagnetic data in Saleh et al. (2013)

triggered the 1995 earthquake of moment magnitude 7.3 occurred at a NNE sinistral strike-slip fault. The extensional deformation accommodated by the relative tectonic movement between the African and Arabian plates as well as the anticlockwise rotation of the Sinai sub-plate caused the 1969 earthquake of moment magnitude 6.2 occurred at a NNW normal fault. No distinctive relationship was recognized between the focal mechanisms, *b*-values, and the state of stress.

To elucidate the nature of the crust and its heterogeneity, the integration of high-quality geophysical data can detail the development of geodynamic processes that generate lithospheric deformations. Based on the available data used in this study's analysis, the current results cannot be extended to distinguish the nature of the crust in the NRS region. Additionally, there is still considerable debate on the evidence of variations in rheological characteristics that are likely to be associated with stress heterogeneities in the Earth's crust. Further studies, based on high-quality data, are required for determining the nature of the Earth's crust in the NRS.

5 Conclusions

This study presents an analysis based on the spatial variations in b -values, moment releases, gravity, and magnetic anomalies, with the aim of investigating the crustal and stress heterogeneities in the NRS region. According to our analysis, it is noteworthy that the region shows the compatibility of gravity anomalies, b -values, and cumulative seismic moment releases where the positive gravity anomalies and high b -values are proportional to higher stress accumulations and vice versa. Gravity analysis shows that the crusts of the Gulf of Aqaba and the Gulf of Suez are not thin enough to compensate for the lack of mass represented by water, implying that the crust in these regions is still thick and rigid; however, the crust in Gulf of Aqaba is relatively thinner and weaker compared to the crust in the Gulf of Suez. In this crust, any topographic load due to excess or deficiency of mass will be supported by the rigidity of the crust and induce lower stress accumulation that is consistent with the distributions of lower cumulative seismic moment releases and low b -values. In the NRS, we observe a regional Bouguer positive anomaly trending along the axial rift of the Red Sea; the anomaly becomes negative toward the western and eastern margins, implying a crust thinning from the shield toward the axis of the Red Sea. As the crust of the Red Sea is thin enough to compensate for the lack of mass represented by the water, the crust is deemed to be weak and not rigid. In this crust, any topographic load due to excess or deficiency of mass will induce high stress accumulation, which is congruent with the distribution of high b -values and comparatively higher seismic moment releases. The NRS also shows short-wavelength gravity and magnetic anomalies with low positive or negative amplitudes that trend mainly along the NW–SE direction, which is parallel to the Red Sea rifting, and the NE–SW direction, which is perpendicular to the Red Sea rifting. These gravitational and magnetic short wavelengths indicate crustal heterogeneities due to mega faults, intruded dikes, and volcanic activity over the trends that are parallel and conjugate to the Red Sea rifting.

The current study shows that the NRS region is dominated by heterogeneities in stress distributions and crustal characteristics. The region shows a crustal thickness change, illustrating that the Moho regional field is the main component of gravity anomalies. Earthquakes with larger magnitudes occur consistently in the Gulf of Aqaba and the mouth of the Gulf of Suez zones and are associated with low b -values, lower seismic moment releases, and negative gravity anomalies. Zones with negative isostatic anomalies, low b -values, and low stress accumulations characterized the older and more stable crust. Earthquakes with relatively smaller magnitudes occur consistently in the central area of the NRS and lead to an increase in stress accumulation and a resulting increase in b -values; this result is coincident with the zones nearby to the isostatic equilibrium in that high isostatic anomalies are likely to be in tandem with relatively weakened or young crust, thus implying magma upwelling or low-velocity zones. However, based on the available data used in our analysis, we can only describe the stress heterogeneities in the Earth's crust and we cannot provide more details on the nature of the crust in the NRS; additional high-resolution geophysical and geological data are required in future studies.

Acknowledgements The authors extend their sincere appreciation to the Deanship of Scientific Research at King Saud University for funding this work through research Group No. RG-1441-320. Generic Mapping Tools developed by Wessel and Smith (1995) were used for most data mapping.

Compliance with Ethical Standards

Conflict of interest The authors declare no potential conflict or competing interests.

References

- Abdelfattah AK, Almadani S, Fnais M, Alfaihi HJ, Al-Arifi N, Al-amri A et al (2019) Rupture characteristics of a small-sized earthquake (MW 4.2), onshore the south Red Sea, Saudi Arabia. *J Afr Earth Sc* 151:315–323
- Abdel-Fattah AK, Mogren SM, Almadani S (2016) Seismicity constraints on stress regimes along Sinai subplate boundaries. *Stud Geophys Geod* 60(2):268–279
- Aki K (1965) Maximum likelihood estimate of b in the formula $\log N = a - bM$ and its confidence limits. *Bull Earthq Res Inst Tokyo Univ* 43:237–239
- Aki K (1966) Earthquake generating stress in Japan for the years 1961 to 1963 obtained by smoothing the first motion radiation patterns. *Bull Earthq Res Inst Univ Tokyo* 44:447–471
- Al-Amri AM (1995) Recent seismic activity in the northern Red Sea. *J Geodyn* 20(3):243–253
- Almalki KA, Betts PG, Ailleres L (2015) The Red Sea–50 years of geological and geophysical research. *Earth Sci Rev* 147:109–140
- Almalki KA, Betts PG, Ailleres L (2016) Incipient seafloor spreading segments: insights from the Red Sea. *Geophys Res Lett* 43(6):2709–2715
- ArRajehi A, McClusky S, Reilinger R, Daoud M, Alchalbi A, Ergintav S, Gomez F, Sholan J, Bou-Rabee F, Ogubazghi G, Haileab B (2010) Geodetic constraints on present-day motion of the Arabian Plate: implications for Red Sea and Gulf of Aden rifting. *Tectonics* 29(3):TC3011
- Badawy A, Abdel-Fattah AK (2006) 2001 August earthquake swarm at Shadwan Island, Gulf of Suez, Egypt. *Geophys J Int* 167(1):288–296
- Balmino G, Vales N, Bonvalot S, Briais A (2011) Spherical harmonic modeling to ultra-high degree of Bouguer and isostatic anomalies. *J Geod* 86:499–520
- Ben-Menahem A, Aboodi E (1971) Tectonic patterns in the northern Red Sea region. *J Geophys Res* 76(11):2674–2689
- Bentor YK (1985) The crustal evolution of the Arabo-Nubian Massif with special reference to the Sinai Peninsula. *Precambr Res* 28(1):1–74
- Bonatti E (1985) Punctiform initiation of seafloor spreading in the Red Sea during transition from a continental to an oceanic rift. *Nature* 316(6023):33–37
- Bonvalot S, Balmino G, Briais A, Kuhn M, Peyrefitte A, Vales N, Biancale R, Gabalda G, Reinquin F (2012) World Gravity Map: a set of global complete spherical Bouguer and isostatic anomaly maps and grids. In EGU general assembly conference abstracts 14:11091
- Bosworth W (2015) Geological evolution of the Red Sea: historical background, review, and synthesis. In: Rasul NM, Stewart ICF (eds) *The Red Sea*. Springer, Berlin, pp 45–78
- Bosworth W, Durocher S (2017) Present-day stress fields of the Gulf of Suez (Egypt) based on exploratory well data: non-uniform regional extension and its relation to inherited structures and local plate motion. *J Afr Earth Sci* 136:136–147
- Bosworth W, Sultan M, Stern RJ, Arvidson RE, Shore P, Becker R (1993) Nature of the Red Sea crust: a controversy revisited: comment and reply. *Geology* 21(6):574–576
- Bosworth W, Huchon P, McClay K (2005) The Red Sea and Gulf of Aden basins. *J Afr Earth Sci* 43(1–3):334–378
- Bridges DL, Gao SS (2006) Spatial variation of seismic b -values beneath Makushin Volcano, Unalaska Island, Alaska. *Earth Planet Sci Lett* 245(1–2):408–415
- Buck R, Martinez F, Steckler MS, Cochran JR (1988) Thermal consequences of lithospheric extension: pure and simple. *Tectonics* 7:213–234
- Chang SJ, Van der Lee S (2011) Mantle plumes and associated flow beneath Arabia and East Africa. *Earth Planet Sci Lett* 302(3–4):448–454
- Chernick MR (1999) *Bootstrap methods: a practitioner's guide*, Wiley Series in Probability and Statistics. Wiley-Interscience Publication, London
- Chu D, Gordon RG (1998) Current plate motions across the Red Sea. *Geophys J Int* 135:313–328
- Cochran JR (1983) A model for development of Red Sea. *Aapg Bull* 67(1):41–69
- Cochran JR (2005) Northern Red Sea: nucleation of an oceanic spreading center within a continental rift. *Geochem Geophys Geosyst* 6(3):34

- Cochran JR, Karner GD (2007) Constraints on the deformation and rupturing of continental lithosphere of the Red Sea: the transition from rifting to drifting. *Geol Soc Lond Special Publ* 282(1):265–289
- Cochran JR, Martinez F (1988) Evidence from the northern Red Sea on the transition from continental to oceanic rifting. *Tectonophysics* 153(1–4):25–53
- Daradich A, Mitrovica JX, Pysklywec RN, Willett SD, Forte AM (2003) Mantle flow, dynamic topography, and rift-flank uplift of Arabia. *Geology* 31(10):901–904
- Davies JH (2013) Global map of solid Earth surface heat flow. *Geochem Geophys Geosyst* 14(10):4608–4622
- Dymet J, Tapponnier P, Afifi AM, Zinger MA, Franken D, Muzaiyen E (2013) A new seafloor spreading model of the Red Sea: magnetic anomalies and plate kinematics. American Geophysical Union, Fall Meeting, abstract #T21A-2512
- Edrik M, Kamer Y, Demircioğlu M, Şeşetyan K (2012) 23 October 2011 Van (Turkey) earthquake. *Nat Hazards* 64:651–665
- Ehrhardt A, Hübscher C (2015) The northern Red Sea in transition from rifting to drifting—lessons learned from ocean deeps. In: Rasul NM, Stewart ICF (eds) *The Red Sea*. Springer, Berlin, pp 99–121
- El-Isa Z, Shanti A (1989) Seismicity and tectonics of the Red Sea and western Arabia. *Geophys J Int* 97(3):449–457
- El Khrepy S, Koulakov I, Al-Arifi N (2016a) Crustal and uppermost mantle structure beneath the continental rifting area of the Gulf of Suez from earthquake tomography. *Tectonophysics* 668:92–104
- El Khrepy S, Koulakov I, Al-Arifi N, Petrunin AG (2016b) Seismic structure beneath the Gulf of Aqaba and adjacent areas based on the tomographic inversion of regional earthquake data. *Universitätsbibliothek Johann Christian Senckenberg, Frankfurt am Main*
- El-Bohoty M, Brimich L, Saleh A, Saleh S (2012) Comparative study between the structural and tectonic situation of the Southern Sinai and the Red Sea, Egypt, as deduced from magnetic, gravity and seismic data. *Contrib Geophys Geod* 42(4):357–388
- El-Nader IA, Hussein HM (2018) The present-day active deformation in the central and northern parts of the Gulf of Suez area, Egypt, from earthquake focal mechanism data. *Nat Hazards* 92(3):1355–1369
- Freund R, Garfunkel Z, Zak I, Goldberg M, Weissbrod T, Derin B, Bender F, Wellings FE, Girdler RW (1970) The shear along the Dead Sea rift. *Philos Trans R Soc Lond Ser A Math Phys Sci* 267:107–130
- Garson MS, Krs M (1976) Geophysical and geological evidence of the relationship of Red Sea transverse tectonics to ancient fractures. *Geol Soc Am Bull* 87(2):169–181
- Gaulier JM, Le Pichon X, Lyberis N, Avedik F, Geli L, Moretti I, Deschamps A, Hafez S (1988) Seismic study of the crust of the northern Red Sea and Gulf of Suez. *Tectonophysics* 153(1–4):55–88
- Ghebream W (1998) Tectonics of the Red Sea region reassessed. *Earth Sci Rev* 45(1–2):1–44
- Girdler RW, Underwood M (1985) The evolution of early oceanic lithosphere in the southern Red Sea. *Tectonophysics* 116(1–2):95–108
- Gomez F, Nemer T, Tabet C, Khawlie M, Meghraoui M, Barazangi M (2007) Strain partitioning of active compression within the Lebanese restraining bend of the Dead Sea Fault (Lebanon and SW Syria). *Geol Soc Lond Spec Publ* 290(1):285–303
- Görgün E (2013) Analysis of the b-values before and after the 23 October 2011 Mw 7.2 Van-Erciş, Turkey earthquake. *Tectonophysics* 603:213–221
- Guennoc P, Pautot G, Coutelle A (1988) Surficial structures of the northern Red Sea axial valley from 23 N to 28 N: time and space evolution of neo-oceanic structures. *Tectonophysics* 153(1–4):1–23
- Gutenberg B, Richter CF (1941) Seismicity of the Earth. *Geol Soc Am Sp Pap* 34:1–133
- Joffe S, Garfunkel Z (1987) Plate kinematics of the circum Red Sea—a re-evaluation. *Tectonophysics* 141(1–3):5–22
- Kalyoncuoğlu UY, Elitok Ö, Dolmaz MN (2013) Tectonic implications of spatial variation of b-values and heat flow in the Aegean region. *Mar Geophys Res* 34(1):59–78
- Kalyoncuoğlu ÜY, Elitok Ö, Dolmaz MN, Anadolu NC (2011) Geophysical and geological imprints of southern Neotethyan subduction between Cyprus and the Isparta Angle, SW Turkey. *J Geodyn* 52(1):70–82
- Kanamori H, Brodsky EE (2001) The physics of earthquakes. *Phys Today* 54(6):34–40
- Khan PK (2005) Mapping of b-value beneath the Shillong Plateau. *Gondwana Res* 8(2):271–276
- Khan PK, Chakraborty PP (2007) The seismic b-value and its correlation with Bouguer gravity anomaly over the Shillong Plateau area: tectonic implications. *J Asian Earth Sci* 29(1):136–147
- LaBrecque JL, Zitellini N (1985) Continuous sea-floor spreading in Red Sea: an alternative interpretation of magnetic anomaly pattern. *AAPG Bull* 69(4):513–524
- Lei X (2003) How do asperities fracture? An experimental study of unbroken asperities. *Earth Planet Sci Lett* 213(3–4):347–359

- Ligi M, Bonatti E, Bosworth W, Cai Y, Cipriani A, Palmiotto C, Ronca S, Seyler M (2018) Birth of an ocean in the Red Sea: oceanic-type basaltic melt intrusions precede continental rupture. *Gondwana Res* 54:150–160
- Lolli B, Gasperini P, Vannucci G (2014) Empirical conversion between teleseismic magnitudes (mb and Ms) and moment magnitude (M_w) at the Global, Euro-Mediterranean and Italian scale. *Geophys J Int* 199(2):805–828
- Lucazeau F (2019) Analysis and mapping of an updated terrestrial heat flow data set. *Geochem Geophys Geosyst* 20(8):4001–4024
- Maden N, Öztürk S (2015) Seismic b-values, bouguer gravity and heat flow data beneath Eastern Anatolia, Turkey: tectonic implications. *Surv Geophys* 36(4):549–570
- Mahmoud S, Reilinger R, McClusky S, Vernant P, Tealeb A (2005) GPS evidence for northward motion of the Sinai Block: implications for E. Mediterranean tectonics. *Earth Planet Sci Lett* 238(1–2):217–224
- Mart Y, Hall JK (1984) Structural trends in the northern Red Sea. *J Geophys Res Solid Earth* 89(B13):11352–11364
- Mart Y, Horowitz A (1981) The tectonics of the Timna region in southern Israel and the evolution of the Dead Sea Rift. *Tectonophysics* 79(3–4):165–199
- Mart Y, Rabinowitz PD (1986) The northern red sea and the dead sea rift. *Tectonophysics* 124(1–2):85–113
- McNutt SR (2005) Volcanic seismology. *Annu Rev Earth Planet Sci* 32:461–491
- Meyer B, Saltus R, Chulliat A (2017) EMAG2: earth magnetic anomaly grid (2-arc-minute resolution) version 3. National Centers for Environmental Information, NOAA, Model, Asheville
- Mitchell NC, Park Y (2014) Nature of crust in the central Red Sea. *Tectonophysics* 628:123–139
- Mitchell NC, Stewart IC (2018) The modest seismicity of the northern Red Sea rift. *Geophys J Int* 214(3):1507–1523
- Mogi K (1963) Some discussions on aftershocks, foreshocks, and earthquake swarms—the fracture of a semi-infinite body caused by an inner stress origin and its relation to the earthquake phenomena. 3. *Bull Earthquake Res Inst Tokyo* 41:615–658
- Mogi K (1967) Effect of the intermediate principal stress on rock failure. *J Geophys Res* 72(20):5117–5131
- Mousavi SM (2017a) Mapping seismic moment and b-value within the continental collision orogenic-belt region of the Iranian Plateau. *J Geodyn* 103:26–41
- Mousavi SM (2017b) Spatial variation in the frequency–magnitude distribution of earthquakes under the tectonic framework in the Middle East. *J Asian Earth Sci* 147:193–209
- Pamukçu O (2016) Geodynamic assessment of Eastern Mediterranean region: a joint gravity and seismic b value approach. *Arab J Geosci* 9(5):360
- Pavlis NK, Holmes SA, Kenyon SC, Factor JK (2012) The development and evaluation of the Earth Gravitational Model 2008 (EGM2008). *J Geophys Res Solid Earth* 117(B4):B04406
- Rihm R, Makris J, Möller L (1991) Seismic surveys in the Northern Red Sea: asymmetric crustal structure. *Tectonophysics* 198(2–4):279–295
- Saleh S, Salk M, Pamukçu O (2013) Estimating Curie point depth and heat flow map for northern Red Sea rift of Egypt and its surroundings, from aeromagnetic data. *Pure Appl Geophys* 170(5):863–885
- Sánchez JJ, McNutt SR, Power JA, Wyss M (2004) Spatial variations in the frequency–magnitude distribution of earthquakes at Mount Pinatubo Volcano. *Bull Seismol Soc Am* 94(2):430–438
- Sandwell D, Garcia E, Soofi K, Wessel P, Chandler M, Smith WH (2013) Toward 1-mGal accuracy in global marine gravity from CryoSat-2, Envisat, and Jason-1. *Lead Edge* 32(8):892–899
- Sandwell DT, Müller RD, Smith WH, Garcia E, Francis R (2014) New global marine gravity model from CryoSat-2 and Jason-1 reveals buried tectonic structure. *Science* 346(6205):65–67
- Scholz CH (1968) Experimental study of the fracturing process in brittle rock. *J Geophys Res* 73(4):1447–1454
- Schorlemmer D, Wiemer S, Wyss M (2004) Earthquake statistics at Parkfield: 1 Stationarity of b values. *J Geophys Res Solid Earth* 109(B12):B12308
- Schorlemmer D, Wiemer S, Wyss M (2005) Variations in earthquake-size distribution across different stress regimes. *Nature* 437(7058):539–542
- Shi Y, Bolt BA (1982) The standard error of the magnitude-frequency b value. *Bull Seismol Soc Am* 72(5):1677–1687
- Sobiesiak M, Meyer U, Schmidt S, Götze HJ, Krawczyk CM (2007) Asperity generating upper crustal sources revealed by b value and isostatic residual anomaly grids in the area of Antofagasta, Chile. *J Geophys Res Solid Earth* 112(B12):B12308
- Stein M, Goldstein SL (1996) From plume head to continental lithosphere in the Arabian-Nubian shield. *Nature* 382(6594):773–778
- Stern RJ (1994) Neoproterozoic (900–550 Ma) arc assembly and continental collision in the East African Orogen. *Ann Rev Earth Planet Sci* 22:319–351

- Stern RJ, Johnson P (2010) Continental lithosphere of the Arabian Plate: a geologic, petrologic, and geophysical synthesis. *Earth Sci Rev* 101(1–2):29–67
- Stern RJ, Johnson PR (2019) Constraining the opening of the Red Sea: evidence from the neoproterozoic margins and cenozoic magmatism for a volcanic rifted margin. In: Rasul NM, Stewart ICF (eds) *Geological setting, palaeoenvironment and archaeology of the Red Sea*. Springer, Cham, pp 53–79
- Sultan M, Becker R, Arvidson RE, Shore P, Stern RJ, El Alfy Z, Guinness EA (1992) Nature of the Red Sea crust: a controversy revisited. *Geology* 20(7):593–596
- Tapponnier P, Dymant J, Zinger MA, Franken D, Afifi AM, Wylie A, Ali HG, Hanbal I (2013) Revisiting seafloor-spreading in the Red Sea: basement nature, transforms and ocean-continent boundary, American Geophysical Union, Fall Meeting 2013, San Francisco, CA, 9–13 Dec, abstract #T12B-04
- Urbancic TI, Trifu CI, Long JM, Young RP (1992) Space-time correlations of b values with stress release. *Pure Appl Geophys* 139(3–4):449–462
- Wang JH (1988) b values of shallow earthquakes in Taiwan. *Bull Seismol Soc Am* 78(3):1243–1254
- Warren NW, Latham GV (1970) An experimental study of thermally induced microfracturing and its relation to volcanic seismicity. *J Geophys Res* 75(23):4455–4464
- Wdowinski S, Bock Y, Baer G, Prawirodirdjo L, Bechor N, Naaman S, Knafo R, Forrai Y, Melzer Y (2004) GPS measurements of current crustal movements along the Dead Sea Fault. *J Geophys Res Solid Earth* 109(B5):B05403
- Wessel P, Smith WHF (1995) New version of the generic mapping tools released. *Eos Trans Am Geophys Union* 76:329
- Wiemer S, Zuñiga FR (1994) ZMAP - A software package to analyze seismicity. *EOS, Trans., Fall Meeting*. 75. AGU, p. 456
- Wiemer S, Katsumata K (1999) Spatial variability of seismicity parameters in aftershock zones. *J Geophys Res Solid Earth* 104(B6):13135–13151
- Wiemer S, Wyss M (2000) Minimum magnitude of completeness in earthquake catalogs: examples from Alaska, the western US and Japan. *Bull Seism Soc Am* 90:859–869
- Wiemer S, McNutt SR, Wyss M (1998) Temporal and three-dimensional spatial analyses of the frequency-magnitude distribution near Long Valley Caldera, California. *Geophys J Int* 134:409–421
- Wyss M (1973) Towards a physical understanding of the earthquake frequency distribution. *Geophys J R Astron Soc* 31(4):341–359
- Wyss M, Stefansson R (2006) Nucleation points of recent mainshocks in southern Iceland, mapped by b-values. *Bull Seismol Soc Am* 96(2):599–608

Publisher's Note Springer Nature remains neutral with regard to jurisdictional claims in published maps and institutional affiliations.